GEOPHYSICAL RESEARCH LETTERS, VOL. 25, NO.17, PAGES 3273-3276, SEPTEMBER 1, 1998

Hybrid simulation of the curved dayside magnetopause during southward IMF

N. Omidi, H. Karimabadi and D. Krauss-Varban

SciberNet Inc., San Diego, CA, and University of California, San Diego

Abstract. Large-scale, 2-D hybrid (fluid electrons, particle ions) simulations have been performed to investigate the macroscopic and the microscopic structure of the dayside (curved) magnetopause during southward IMF. It is found that in addition to the formation of an X-line at the subsolar point, other X lines are formed at higher latitudes. The locations of these X lines are asymmetric with respect to the magnetic equator, and the resulting plasmoids have different sizes. The thickness of the magnetopause varies considerably as a function of latitude. In addition, the spatial scales associated with the plasma variations across the magnetopause are considerably different than those associated with the field variations. The rotational (current) layer exhibits a linear polarization and does not match the jump conditions of any known discontinuity. Instead, the topology of the magnetic field lines, determines the spatial scale and the polarization of the current layer.

Introduction

It was suggested by Dungey [1961] that magnetic reconnection leads to a strong coupling between the solar wind and the magnetospheric fields and plasma during periods of southward IMF. Other early investigations (e.g. Levy et al., 1964) led to a more detailed structure for the magnetopause consisting of a number of MHD waves and discontinuities. Over the past three decades, continued research in this area has led to many insights and discoveries. For example, observations by Russell and Elphic [1978] of flux transfer events (FTE) led to a number of time dependent patchy reconnection models (e.g. Lee and Fu, 1985; Scholer, 1988; La Belle-Hamer et al., 1988). Observations have also shown magnetopause structures that are consistent with time stationary models (e.g. Sonnerup et al., 1981). In general, the magnetopause is more than a single discontinuity and exhibits structures which vary from electron to many ion characteristic time and spatial scales (see e.g. Elphic, 1989).

In the past, hybrid (fluid electrons, kinetic ions) simulation studies of the magnetopause have concentrated on various topics such as solutions to the Riemann problem (e.g. Lin and Lee, 1994; Omidi and Winske, 1995), structure of rotational and tangential discontinuities and intermediate shocks (e.g., Goodrich and Cargill, 1991; Krauss-Varban et al., 1995; Cargill and Eastman, 1991; Karimabadi, 1995), as well as, resistive and viscous diffusion due to microscopic and macroscopic instabilities (e.g. Gary and Sgro, 1990; Thomas and Winske, 1993; Winske and Omidi, 1995). In a global hybrid simulation of solar wind interaction with a dipole Swift [1995] showed the formation of magnetic islands at the magnetopause. In this paper, we present initial results from a large-scale 2-D hybrid simulation of the dayside magnetopause during a period of southward IMF. The model magnetopause is formed through the interaction between a solar wind type plasma and a dipole field which also results in the formation of a bow shock. This model allows us to investigate the macro- as well as the micro- structure of the magnetopause in a coupled and self-consistent manner. Due to the 2-D nature of the simulation and the parameters chosen, the size and locations of the various boundaries formed in the run are different from their terrestrial counterpart.

Paper number 98GL02484.
0094-8534/98/98GL-02484$05.00

Simulation Results

The results shown here are from a 2-D hybrid code where the plane of simulation (X–Y) corresponds to the noon-midnight meridian plane. The three components of particle velocities and electromagnetic fields are retained in the model. The simulation box is 350×600 c/ω_p long in the X and Y directions, respectively, and the cell size is 1×1 c/ω_p. Here, c/ω_p is the ion inertial length in the solar wind (~ 100 km). Initially, the box is filled with 8.4 million macro-particles representing the solar wind ions. In addition, solar wind plasma is continuously injected from the left hand boundary ($X = 0$, $0 \leq Y \leq 600$) along the X direction. The electron and ion beta of this plasma are 0.5 each (beta is the ratio of kinetic to magnetic pressure) and the solar wind flow velocity is 4 V_A, where V_A is the Alfven velocity. Throughout the run, more than 17 million particles are processed with about 11 million in the box at the end of the run. The solar wind magnetic field (IMF) is in the X-Y plane and mostly southward, making an angle of 85° with the X-axis. The magnetic field of the Earth is modeled as a line dipole where the field strength drops off as $1/r^2$ (see e.g. Ogino, 1993). Because we are only investigating the dayside of the magnetopause, the center of the dipole is located outside and to the right of the simulation box with X and Y coordinates of $(420, 300)$ c/ω_p. The dipole moment is chosen such that the associated field strength at the point (X=120, Y=300) is the same as the IMF magnitude. A spatially uniform resistivity corresponding to a resistive scale length of 0.5 c/ω_p is present in the model. Floating boundary conditions are assumed for the electromagnetic fields on the top, bottom, and the right hand walls, while the left hand wall maintains a fixed field corresponding to the solar wind. Particles are allowed to leave the box in

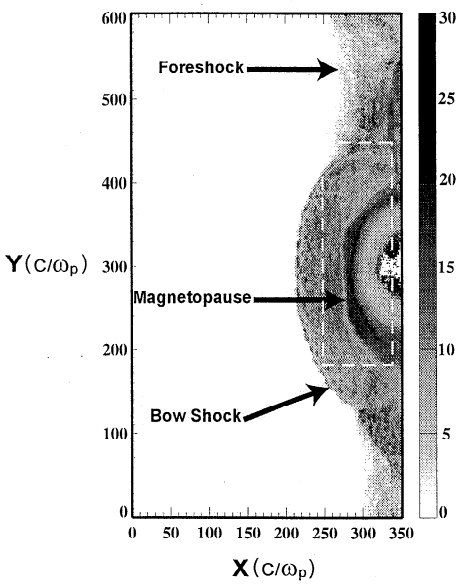

Figure 1. Intensity plot of ion temperature as a function of X and Y at the end of the simulation run illustrating the shape and position of the foreshock, bow shock and the magnetopause.

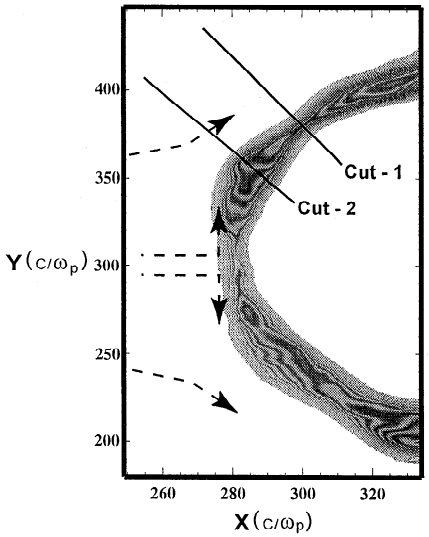

Figure 2. Magnetic field lines (in the X-Y plane) within the magnetopause are shown by plotting contours of constant z-component of the vector potential. The dashed arrows show the general flow pattern in the magnetosheath and the subsolar magnetopause.

all four directions. The presence of plasma with magnetospheric or ionospheric origin has not been accounted for in the model, and as a result, all the plasma present in the magnetosphere is of solar wind origin.

Figure 1 shows the intensity plot of ion temperature as a function of X and Y at the end of the run ($\Omega_p\ t\ =\ 100$ where Ω_p is the proton gyrofrequency). In the figure, the arrows point to the foreshock, bow shock, and the magnetopause with the shocked plasma corresponding to the magnetosheath. The presence of tenuous, energetic, backstreaming ions in the foreshock leads to an artificial increase in the temperature, making it a good diagnostic tool for visualizing this region (N. Omidi et al., submitted to *J. Geophys. Res*, 1998). It can be seen that all of the backstreaming ions originate from the quasi-parallel portion of the bow shock only. The curved magnetopause layer can be seen as a region with its temperature enhanced above the magnetosheath level. Note that because of the absence of magnetospheric plasma, the temperature within the magnetosphere is considerably below what it normally is. It is evident from this figure that the thickness of the magnetopause as measured by the associated temperature enhancement, varies considerably with latitude. This variation is not a monotonically increasing or decreasing function of the latitude and is asymmetric with respect to the magnetic equator.

To investigate the topology of the magnetic field lines within the magnetopause, Figure 2 shows the magnetic field lines in the magnetopause region. Also shown in Figure 2 are a number of arrows illustrating the general flow pattern of the plasma within the magnetosheath and the magnetopause layer. It is evident that magnetic reconnection has taken place at more than one location along the magnetopause surface. One X line is seen near the subsolar point along with two additional ones at northern and southern latitudes. The reconnection in the northern hemisphere has taken place at a higher latitude leading to the formation of two large magnetic islands. On the other hand, the X line in the southern hemisphere occurs at a lower latitude leading to the formation of a smaller island. The presence of a spatially uniform resistivity in the model allows for the tearing instability to be operative at the magnetopause leading to the formation of multiple islands and X lines (e.g. Shi et al., 1988). As can be seen however, the amplitude of the excited modes are not symmetric with respect to the magnetic equator. This asymmetric behavior is attributed to the turbulent nature of the magnetosheath plasma which causes considerable variations in the local direction of the magnetic field.

To examine the microstructure of the magnetopause in this simulation, Figures 3 and 4 show field and plasma variations along the two lines labeled cut-1 and

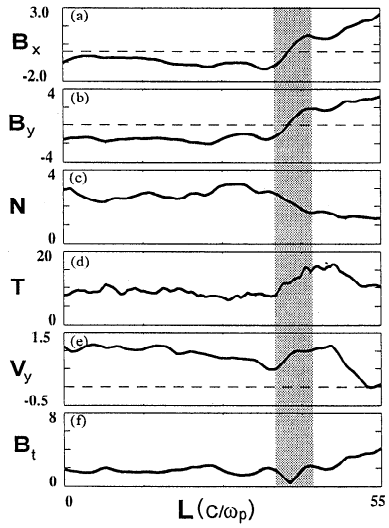

Figure 3. Panels (a)-(f) show the X and the Y components of magnetic field, ion density and temperature, the Y component of ion velocity and the total magnetic field along Cut-1 shown in Figure 2.

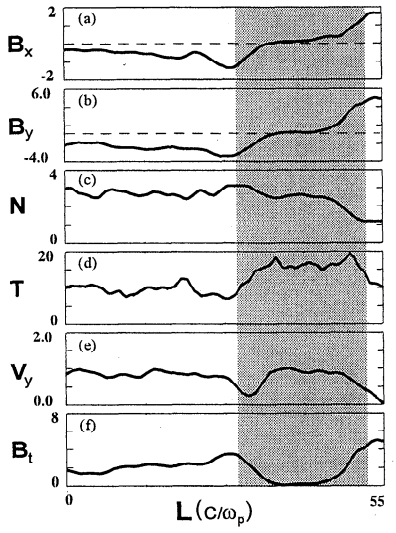

Figure 4. Same as Figure 3 except the trajectory is along Cut-2 shown in Figure 2.

cut-2 (in Figure 2) respectively. These two cuts have been selected to illustrate the magnetopause structure near an X line as well as within a plasmoid. The figures show from top to bottom, the X and Y components of the magnetic field, the ion density and temperature, the Y component of ion velocity, and the total magnetic field, respectively. Here the magnetic field is normalized to the magnitude of IMF, the density and temperature are normalized to their corresponding values in the solar wind, and velocity is normalized to the Alfven speed in the solar wind. Note that the abscissas in Figures 3 and 4 represent the length (L) along the cuts 1 and 2 with L=0 corresponding to the upstream (of the current layer) side. The shaded regions correspond to the width of the rotational (i.e. current) layer. It is evident from Figure 3 that the width of the rotational layer is about 6.5 c/ω_p which represents 10 local ion inertial lengths. One of the interesting aspects of the rotational layer is that it is linearly polarized with no systematic variations in B_z observed within the layer. As a result, the total magnetic field strength exhibits a dip across the layer. This behavior is in contrast with the theoretical studies of rotational discontinuities (RD) in isolation which normally have a circular/elliptical polarization (e.g., Goodrich and Cargill, 1991; Krauss-Varban et al., 1995). Observations of rotational discontinuities in the solar wind and at the magnetopause have shown many examples of circularly polarized RDs (e.g. Neugebauer, 1989; Berchem and Russell, 1982). However, there are also numerous examples of field rotations at the magnetopause that are linearly polarized (e.g. Song et al. 1989).

The linear nature of the field rotation in Figure 3 is not the only departure from the well known properties of isolated RDs. For example, it is evident from panel (c) that the density decreases within the current layer leading to a 50% drop across the layer. This decrease continues well beyond the end point of cut-1 (i.e. L=55) leading to magnetospheric densities of 5-10% that of the solar wind. We have not been able to match the jump in the field and plasma quantities to that of RDs or intermediate shocks. Panel (d) shows a rise in temperature which begins at the upstream edge of the rotational layer and extends well beyond the shaded region. It can be seen in panel (e) that V_y is constant for $0 \leq L \leq 18$ and then it begins to decrease reaching a minimum at the upstream edge of the rotational layer. Like temperature, V_y increases within the current layer and stays high well beyond it.

Examination of Figure 4 shows both similarities and differences in comparison to Figure 3. For example, the field rotation remains linearly polarized, the density drops within the current layer, the temperature begins to increase at the edge of the current layer , and V_y shows a minimum at about the same point. In contrast, the current layer is thicker by about a factor of 4 and has the same width as the region of enhanced temperature. The larger width of the current layer is consistent with a trajectory through a plasmoid. Thus, the thickness of the current layer is determined by the large-scale topology of the magnetic field lines (i.e. the size of the plasmoid), as opposed to any characteristic length scales such as ion gyroradius or inertial length. Normally, magnetic field rotations at the magnetopause are thought to be associated with an RD or intermediate shock. However, such an assertion is clearly not warranted in this case and would neglect major topological differences such as closed magnetic field lines within the rotational layer. In general, the rotation of the magnetic field at the magnetopause may be associated with either an RD/intermediate-shock or a plasmoid and the physical characteristics of the two could be considerably different.

In addition to magnetic topology, plasma transport also affects the microstructure of the magnetopause and can explain a number of features observed in Figures 3 and 4. For example, the characteristics of V_y described above can be understood by considering the flow pattern in the magnetosheath and the boundary layer. In the subsolar region, the magnetosheath flow is essentially along the X-direction (see Figure 2). Upon entering the reconnection region this plasma is accelerated in the Y direction, originating the boundary layer. As a result of this acceleration, only a small fraction of plasma is observed to enter the magnetosphere, and most of it is transported to higher latitudes. At higher latitudes, flow diversion by the bow shock results in the magnetosheath having a finite velocity in the $+/-$ Y directions at northern and southern hemispheres, respectively. This flow pattern causes a gradient in magnetosheath V_y which becomes more pronounced near and upstream of the magnetopause because the flow lines closer to the magnetopause originate at lower latitudes downstream of the shock. In other words, as we move along the cuts-1 or 2 we intersect flow lines originating from points closer and closer to the nose of the bow shock which also correspond to smaller V_y. This explains the decrease in V_y seen upstream of the current layer in Figures 3 and 4. The observed increase in V_y within and downstream of the current layer is associated with both local entry and acceleration of magnetosheath plasma, as well as plasma transport from lower latitudes. It is this latter, non-local, effect which we believe leads to a lack of correspondence between spatial scales associated with magnetic field rotation and plasma variations across the magnetopause. Finally, it is interesting to note that plasma entry into the high latitude X line occurs in an asymmetric fashion and, as a result, the plasma may not necessarily be jetted in both

directions away from the X line. In the specific case of Figure 2 evidence of plasma acceleration is present only on the higher latitude side of the (northern) X line but not its lower latitude side.

Summary

The coupled macroscopic and microscopic structure of the dayside magnetopause, during a period of southward IMF, is investigated via a 2-D hybrid simulation. The large-scale structure of the magnetopause is dominated by the formation of multiple X lines and plasmoids of different sizes. As a result, the thickness of the magnetopause varies considerably with latitude. The presence of an X line near the subsolar point and the acceleration of plasma towards higher latitudes lead to the formation of the low latitude boundary layer. Local entry and acceleration of ions at higher latitudes further enhances the boundary layer plasma. Although it is customary to associate the magnetic field rotation at the magnetopause with either an RD or an intermediate shock, the rotational layer in the simulation does not exhibit properties that are consistent with either of these discontinuities. Instead, both the polarization and the spatial scale associated with the field rotation are determined by the topology of the magnetic field lines. In particular, the rotational layer is shown to be linearly polarized with thicknesses of around 10 local ion inertial lengths near an X line, and about 4 times thicker within a plasmoid.

Acknowledgment. This work was supported by the NASA Space Physics Theory Program and NSF grant ATM-9526002 at SciberNet, Inc. N. Omidi's work was performed under the auspices of California Space Institute at UCSD. Computing and data analysis were performed on the desktop supercomputers at SciberNet, Inc.

References

Berchem, J., and C. T. Russell, Magnetic field rotation through the magnetopause: ISEE 1 and 2 observations, *J. Geophys. Res., 87,* 8139–8148, 1982.

Cargill, P. J., and T. E. Eastman, The structure of tangential discontinuities: 1. Results of hybrid simulations, *J. Geophys. Res., 96,* 13,763 13,779, 1991.

Dungey, J. W., Interplanetary magnetic field and the auroral zones, *Phys. Rev. Lett., 6,* 47, 1961.

Elphic, R. C., Magnetopause structure and dynamics, *GEM report of the workshop on magnetopause and boundary physics,* 13–23, 1989.

Gary, S. P., and A. G. Sgro, The lower hybrid drift instability at the magnetopause, *Geophys. Res. Lett., 17,* 909, 1990.

Goodrich, C. C., and P. J. Cargill, An investigation of the structure of rotational discontinuities, *Geophys. Res. Lett., 18,* 65–68, 1991.

Karimabadi, H., Physics of intermediate shocks: A review, *Adv. Space Res., 15,* 507–520, 1995.

Krauss-Varban, D., H. Karimabadi, and N. Omidi, Kinetic structure of rotational discontinuities: Implications for the magnetopause, *J. Geophys. Res., 100,* 11,981–11,999, 1995.

La Belle-Hamer, A. L., Z. F. Fu, and L. C. Lee, A mechanism for patchy reconnection at the dayside magnetopause, *Geophys. Res. Lett., 15,* 152–155, 1988.

Lee, L. C., and Z. F. Fu, A theory of magnetic flux transfer at the Earth's magnetopause, *Geophys. Res. Lett., 12,* 105–108, 1985.

Levy, R. H., H. E. Petschek, and G. L. Siscoe, Aerodynamic aspects of the magnetospheric flow, *AIAA J., 2,* 2065, 1964.

Lin, Y., and L. C. Lee, Structure and reconnection layers in the magnetopause, *Space Sci. Rev., 65,* 59, 1994.

Neugebauer, M., The structure of rotational discontinuities, *Geophys. Res. Lett., 16,* 1261–1264, 1989.

Ogino, T., Two-dimensional MHD code, in computer space plasma physics: Simulation techniques and software, eds. H. Matsumoto and Y. Omura, p. 161, Terra Scientific Publishing Company, Tokyo, 1993.

Omidi, N., and D. Winske, Structure of the magnetopause inferred from 1-D hybrid simulations, *J. Geophys. Res., 100,* 11,935–11.955, 1995.

Russell, C. T., and R. C. Elphic, Initial ISEE magnetometer results: Magnetopause observation, *Space Sci. Rev., 22,* 681, 1978.

Scholer, M., Magnetic flux transfer at the magnetopause based on single X line bursty reconnection, *Geophys. Res. Lett., 15,* 291–294, 1988.

Shi, Y., C. C. Wu, and L. C. Lee, A study of multiple X line reconnection at the dayside magnetopause, *Geophys. Res. Lett., 15,* 295, 1988.

Song, P., C. T. Russell, N. Lin, R. J. Strangeway, J. T. Gosling, M. Thomson, T. A. Fritz, D. G. Mitchell, and R. R. Anderson, Wave and Particle Properties of the subsolar magnetopause, *Phys. of Space Plasmas, 89,* SPI Conference Proceedings and Reprint Series, 463, eds. T. Chang, G. Crew, and J. Jasperse, Scientific Publishers, Inc, Cambridge, MA, USA, 1989.

Sonnerup, B. U. Ö., G. Paschman, I. Papamastorakis, N. Sckopke, G. Haerendel, S. J. Bame, J. R. Asbridge, J. T. Gosling, and C. T. Russell, Evidence for magnetic field reconnection at the Earth's magnetopause, *J. Geophys. Res., 86,* 10,049–10,067, 1981.

Swift, D. W., Use of a hybrid code to model the Earth's magnetosphere, *Geophys. Res. Lett., 22,* 311, 1995.

Thomas, V. A., and D. Winske, Kinetic simulations of the Kelvin-Helmholtz instability at the magnetopause, *J. Geophys. Res., 98,* 11425, 1993.

Winske, D., and N. Omidi, Diffusion at the magnetopause: Hybrid simulations, *J. Geophys. Res., 100,* 11,923–11,933, 1995.

H. Karimabadi, D. Krauss-Varban, and N. Omidi, SciberNet, Inc., 5414 Oberlin Drive, Suite 251, San Diego, CA 92121. (e-mail: omidi@scibernet.com; homa@scibernet.com; varban@scibernet.com)

(Received April 12, 1998; revised June 15, 1998; accepted June 17, 1998.)